Novel $CrFeCoNiSi_6$/Si System for Boron Removal from Metallurgical Silicon Feedstock

Reference:
M. Xiang; Z. Han; Y. Wang, et al., Novel $CrFeCoNiSi_6$/Si System for Boron Removal from Metallurgical Silicon Feedstock. Industrial & Engineering Chemistry Research 2022, 61 (9), 3412-3417.

ISSN 1520-5045 (2022), Copyright © 2022 American Chemical Society. All rights reserved
Full text (Publisher's DOI): https://doi.org/10.1021/acs.iecr.1c04930
Received 21 December 2021; Received in revised form 12 February 2022; Accepted 18 February 2022

A novel $CrFeCoNiSi_6$/Si system for boron removal from metallurgical silicon feedstock

Mengqi Xiang[a], Zike Han[b], Ye Wang [a1*], Wenxiang Tang [a], Zhiyuan Chen [c], Wenhui Ma [d], Kazuki Morita [e]

[a] School of Chemical Engineering, Sichuan University, Chengdu, 610065, Sichuan, P. R. China

[b] Zhejiang Huayou Cobalt Co., Ltd., 324012, Zhejiang, P. R. China

[c] Flemish Institute for Technological Research (VITO), Boeretang 200, 2400 Mol, Belgium

[d] National Engineering Laboratory of Vacuum Metallurgy, Kunming University of Science and Technology, 650093, Yunnan, P. R. China

[e] Department of Material Engineering, The University of Tokyo, 7-3-1 Hongo, Bunkyo-ku, Tokyo 113-8656, Japan

Abstract:

Based on the synergy of impurity removal and metal boride formation, HEA (CrFeCoNi) solvent was used to remove B from metallurgical-grade Si. With Si purification by Si/ $CrFeCoNiSi_6$(HEAs) system, the compounds of HEAs and CrB_2 were found by using energy-dispersive X-ray spectroscopy (XRD), while the mechanical properties of the HEA were enhanced by doping B. During the directional solidification process, the solid solubility (~1600 ppmw) and segregation coefficient (~0.07) of B in the Si/HEAs system were observed. As cooling rate and the mass ratio of Si to the HEA decreased, the diffusion velocity of B increased accordingly. The results showed that HEAs are effective as solvents for B removal.

Introduction

The production of solar-grade polycrystalline Si using metallurgical methods is advantageous due to its low cost and environmental friendliness, but it remains challenge to remove B from metallurgical-grade Si[2-3]. Removal of B is limited using conventional metallurgical methods due to its high separation coefficient with Si (0.9) and low vapor pressure. However, alloy-refining methods, combined with transition

[1*] Corresponding author.
E-mail address: wangye@scu.edu.cn (Ye Wang).

[2] [] Chen, H.; Morita, K.; Ma, X.; Chen, Z.; Wang, Y. Boron Removal for Solar-Grade Silicon Production by Metallurgical Route:A Review. *Sol. Energy Mater. Sol. Cells* **2019**, *203 (September)*, 110169.

[3] [] Zhao Ding.; Hao Li.; Leon Shaw. New insights into the solid-state hydrogen storage of nanostructured $LiBH_4$-MgH_2 system. *Chemical Engineering Journal.* **2020**, *385*, 123856.

metal additives, can significantly increase the B removal efficiency[4-5].

Compared with Si-Al alloy solvent, HEA can recycle with a stable phase - $CrFeCoNiSi_6$(HEAs) until the B saturated due to high entropy property and stratification phenomenon with pure Si after directional solidification. Moreover, both of remove efficiency and purification rate of B are higher than that of Si-Al alloy, the energy consumption can be offset[6-7]. In a directional solidification growth of polycrystalline Si ingot, two layers will be introduced to facilitate the separation of Si and HEAs/Si due to low Gibbs formation energy of HEAs, so as to realize the efficient utilization and recycling of HEAs/Si layer. Thus, HEAs as a solvent alloy not only can remove impurities from Si, but also will appreciate in value due to enhance its own mechanical properties by B and Si adding.

Results and discussion

This paper introduces the method of preparing the $CrFeCoNiSi_x$ alloy by analytical reagents as raw materials. 1.3 g of Cr, Fe, Co, Ni, and 4.0 g of metallurgical-grade Si powder were mixed uniformly and then placed in a graphite crucible to prepare (Table 1). The furnace cavity of a vertical tubular furnace was heated to 1450 °C with a heating rate of 10 $°C \cdot min^{-1}$. Then the graphite crucible was placed into the furnace and kept in a molten state for 1 hour under Ar atmosphere. Subsequently, the temperature was reduced to a set temperature. The purpose of decrease the temperature is separate HEAs and pure Si in solidification. In the meanwhile, the changes of impurity phases from liquid and solid phase were investigated from above liquidus to below solidus during different temperatures (900-1450°C) using the directional solidification method. The slower the cooling rate, the better the phase separation. After 3 hours, the crucible was quenched and cut in half lengthwise using a diamond wire-cutting machine and polished for EDS analyses.

Table 1. Molar ratio of Cr-Fe-Co-Ni-Si alloy used in the experiments.

[4][] Lei, Y.; Ma, W.; Sun, L.; Dai, Y.; Morita, K. B Removal by Zr Addition in Electromagnetic Solidification Refinement of Si with Si-Al Melt. *Metall. Mater. Trans. B Process Metall. Mater. Process. Sci.* **2016**, *47 (1)*, 27–31.

[5][] Lei, Y.; Ma, W.; Sun, L.; Wu, J.; Dai, Y.; Morita, K. Removal of B from Si by Hf Addition during Al–Si Solvent Refining Process. *Sci. Technol. Adv. Mater.* **2016**, *17* (1), 12–19.

[6][] Seol, J. B.; Bae, J. W.; Li, Z.; Chan Han, J.; Kim, J. G.; Raabe, D.; Kim, H. S. Boron Doped Ultrastrong and Ductile High-Entropy Alloys. *Acta Mater.* **2018**, *151*, 366–376.

[7][] Chin-You Hsu; Jien-Wei Yeh; Swe-Kai Chen; Tao-Tsung Shun. Wear resistance and high-temperature compression strength of Fcc CuCoNiCrAl0.5Fe alloy with boron addition. *Metall. Mater. Trans. A, Phys. Metall. Mater. Sci.* **2004**, *35* (5), 1465–1469.

	Cr	Fe	Co	Ni	Si
$CrFeCoNiSi_x$ alloy	1	1	1	1	24
$CrFeCoNiSi_6$ alloy	1	1	1	1	6

The EDS images of samples were divided into bright and gray phases in **Figs. 1(a)–(c)**. Columnar dendritic were appeared and became finer with increasing temperature. This phenomenon could be attributed to the initial nucleation of the dendritic segregation during the slow cooling process, and consequent precipitation of fine crystal branches during the quenching process.

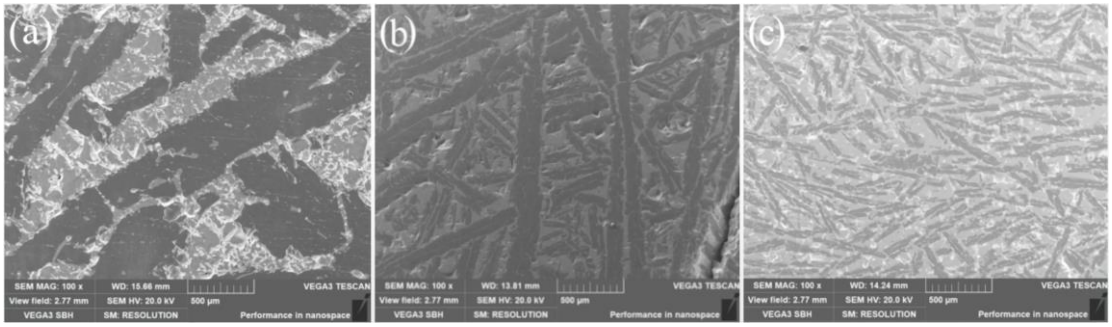

Fig. 1. 100x SEM images of the alloy at different temperatures: (a) 900 ℃; (b) 1350 ℃; (c) 1450 ℃.

EDS surface scanning and point scanning (Fig. 2) were further investigated to confirm the relationship between the composition of each phase and the temperature. Gray and bright phases represent the pure Si and HEA phase respectively. The dark region was Cr-rich phase with a composition of Cr_2Si_3, while the light region was enriched with Fe and Co, the proportion of Si was close to 60%.

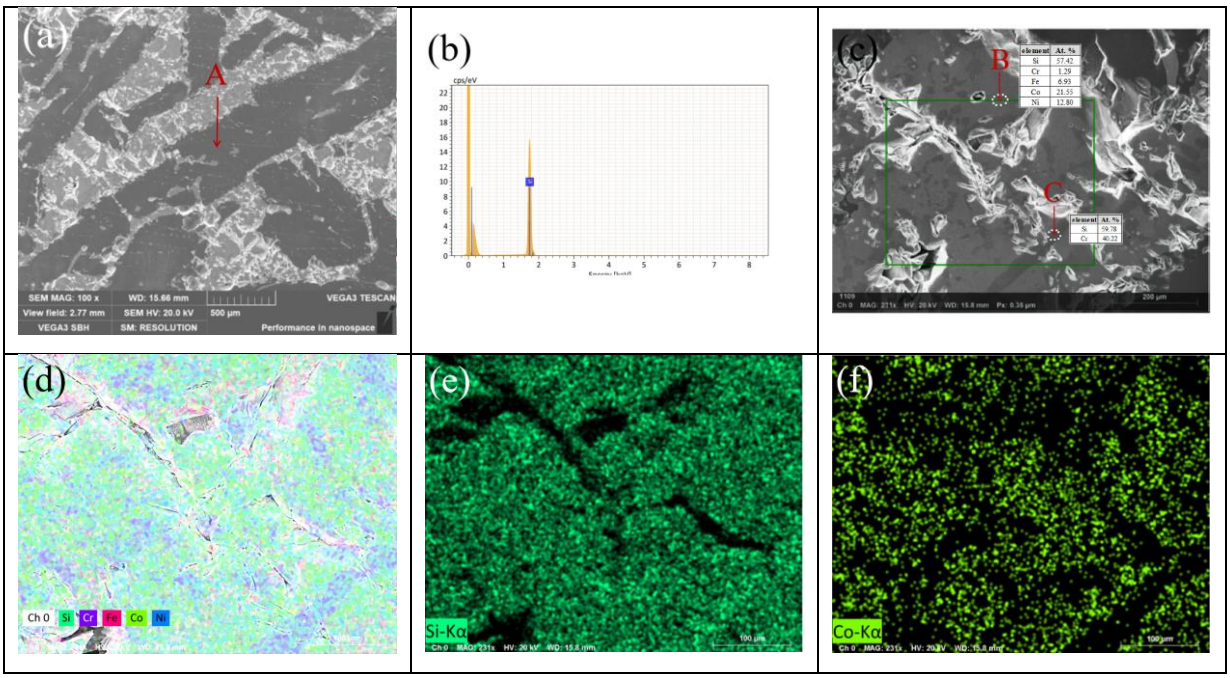

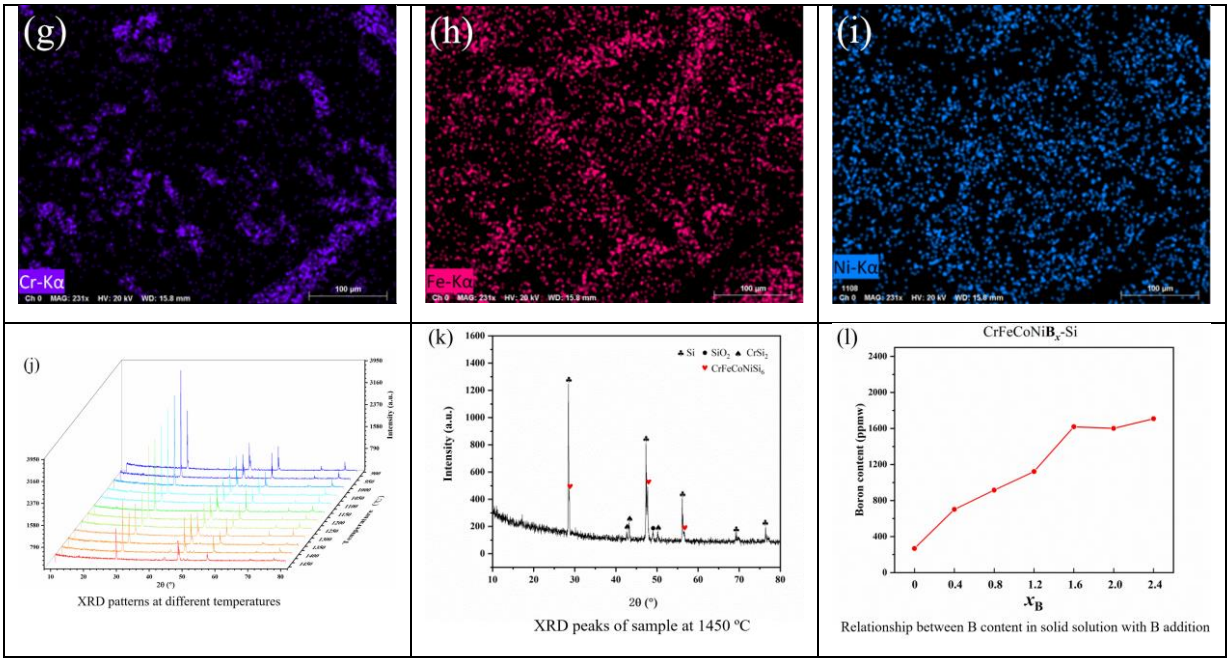

Fig. 2. The EDS results of samples of Fig. 1(a)

(a) SEM; (b) energy spectrum of point A; (c) partial enlargement of point A; (d) element mapping; (e) Si; (f) Co; (g) Cr; (h) Fe ; (i) Ni mapping; (j) XRD patterns; (k) XRD peaks of sample at 1450 ºC; (l) Relationship between B content in solid solution with B addition

HEAs regions were mainly Si-Cr compounds and solid-solution phases during 900-1150 °C. The solid-solution phase exhibited obvious component segregation. **Table 2** lists the EDS point scanning results. The compositions of the Cr-rich phase were Cr_2Si_3 or $CrSi_2$, which is related to the negative mixing enthalpy of Cr-Si. The solid-solution phases were depleted of Cr because they were mainly present in the Cr-rich phase, leading to the observations of Co, Fe, and Ni segregation. The amount of Si in the solid-solution phase was always stable at approximately 60 at.%, and did not change by changing metal elements. This discovery could realize recycling of the $CrMnCoNiSi_6$ as a B removal alloy solvent.

Table 2. Composition of different microstructure areas at different temperatures

Temperature	Cr-poor phase (at. %)					Cr-rich phase (at. %)				
	Si	**Cr**	Fe	Co	Ni	Si	**Cr**	Fe	Co	Ni
900 °C	57.42	**1.29**	6.93	21.55	12.80	59.78	**40.22**			
950 °C	60.37	**1.30**	10.53	10.68	17.12	64.47	**35.53**			
1000 °C	63.48	**0**	7.75	14.65	14.12	64.28	**35.72**			
1050 °C	57.78	**1.21**	8.12	19.08	13.82	58.39	**41.61**			
1100 °C	60.12	**1.18**	7.95	16.42	14.33	63.13	**36.87**			
1150 °C	56.09	**1.12**	6.41	23.70	12.68	60.90	**39.10**			

1200 °C	58.55	**1.55**	6.68	20.82	12.40	61.39	**16.63**	4.31	10.77	6.91
1250 °C	62.70	**5.52**	19.11	5.76	7.02	57.44	**11.27**	6.99	14.37	9.92
1300 °C	61.00	**4.28**	11.46	13.23	10.04	59.94	**22.26**	6.29	5.99	5.52
1350 °C	61.59	**2.20**	24.81	6.03	5.37	56.89	**16.03**	5.67	13.25	8.15
1400 °C	61.17	**2.10**	27.79	4.33	4.61	56.65	**14.24**	6.30	14.07	8.75
1450 °C	60.57	**2.83**	25.58	6.02	4.99	57.30	**18.09**	5.19	12.26	7.15

During the 1200-1450 ºC range, the Si-Cr phases were replaced by a Cr-rich solid-solution phase in the HEA regions. Cr, Fe, Co, and Ni exhibited different degrees of segregation in these regions, especially Cr and Fe. A highly enriched region of Cr as a single metal element was not found. Si was evenly distributed in these regions. The reason of mass transfer of Fe，Co and Ni between the Cr-poor phase and Cr-rich phase might be the transition of solid solution phase during high temperature.

Single-phase HEAs also exhibited segregation on the basis of literatures published[8-9]. The entire HEAs region was scanned, for understanding the solubility of Si and the composition of metal elements, as shown in **Table 3**. The approximate composition of the alloy could be inferred as $CrFeCoNiSi_6$(HEAs). The X-ray diffraction (XRD) patterns at different temperatures showed unchangeable solid-solution phase of HEAs with temperature varies (**Fig. 2j, 2k)**.

Table 3. Average composition of solid solution phase at different temperatures

Temperature	Mole fraction (%)				
	Si	Cr	Fe	Co	Ni
900 °C	62.15	6.95	10.17	10.57	10.17
950 °C	62.90	9.02	9.59	9.09	9.40
1000 °C	62.12	2.04	12.91	10.87	12.06
1050 °C	59.95	6.92	13.02	9.47	10.64
1100 °C	60.12	9.45	10.08	10.29	10.07
1150 °C	63.31	10.39	8.89	9.09	8.32
1200 °C	58.85	7.81	11.66	10.76	10.92
1250 °C	62.61	7.54	10.31	8.73	10.80

[8] [] Chen, H.; Ren, Y. S.; Ma, W. H.; Zeng, Y. Distribution behaviour of boron between ZrTiHfCuNi high entropy alloy and silicon. *Separation and Purification Technology.* **2021**, 271.

[9] [] Wang, J.; Wu, S.; Fu, S.; Liu, S.; Yan, M.; Lai, Q.; Lan, S.; Hahn, H.; Feng, T. Ultrahigh Hardness with Exceptional Thermal Stability of a Nanocrystalline CoCrFeNiMn High-Entropy Alloy Prepared by Inert Gas Condensation. *Scr. Mater.* **2020**, *187*, 335–339.

1300 °C	59.12	10.30	9.49	11.29	9.81
1350 °C	62.77	9.30	9.39	9.29	9.25
1400 °C	57.88	9.75	11.37	10.29	10.71
1450 °C	58.45	9.63	10.92	10.52	10.48
Mean	**60.85**	**8.23**	**10.65**	**10.02**	**10.22**

To investigate the solid solubility of B and boride formation in the HEAs, 1.3 g of Cr, Fe, Co, Ni powder with equimolar quantities, 4.0 g of Si powder, and 0.025, 0.05, 0.075, 0.1, 0.125, 0.15 g of B powder were mixed respectively and then placed in a graphite crucible, heated by a vertical tubular furnace, and mixtures of CrFeCoNiB*x*-Si were obtained (x = 0.4, 0.8, 1.2, 1.6, 2.0, and 2.4). The furnace cavity was heated to 1450 °C, and the graphite crucible was placed inside for 2 hours. Subsequently, the temperature was reduced to a set temperature with a cooling rate of 10 °C·min $^{-1}$, and then remained constant for 4 hours. The whole process was under Ar atmosphere. The crucible was cut and polished for SEM-EDS analysis. The B in the sample was detected by ICP-OES after dissolving the Si with HCl and HNO_3. The amount of B was calculated as follows:

$$C_B = \frac{n \times V}{\left(m - m_{\text{residue}}\right) \div \left(1 - w_{Si}\right)} \quad (1)$$

where C_B is the mass fraction of B in the alloy (ppmw), n is the ICP-OES result (μg/mL), V is the volume of the solution (mL), m and m_{residue} are the sampling mass and the filter residue mass, g; and w_{Si} is the mass fraction of Si in the HEAs, which is approximately 0.428.

The amount of B in the solid-solution phase tended to be stable after increasing to ~1600 ppmw, which was much lower than the initial B amount (4700-28000 ppmw), as shown in **Fig. 2(l)**. The solubility of B with respect to the solid-solution phase was limited to ~1600 ppmw. The reaction of excess B and HEAs can also be proved by the insoluble formation of chromium boride when dissolving the sample with HF+HNO_3.

Figs. 3(a)–(h) show that the distributions of B and Cr are obviously related. The compound of two points was CrB_3 when Si was dissolved. The ratio of Cr to B in the raw materials was in the 2-3 range. B existed in the form of CrB_2 and CrB_3 in the CrFeCoNi$B_{2.4}$-Si system from EDS results. CrB_2 was precipitated in strips during the holding stage (1450 °C) due to its high melting point (1760 °C), and CrB_3 was distributed in blocks. Thus, excess B in the system formed CrB_x with Cr, while other

borides were not formed.

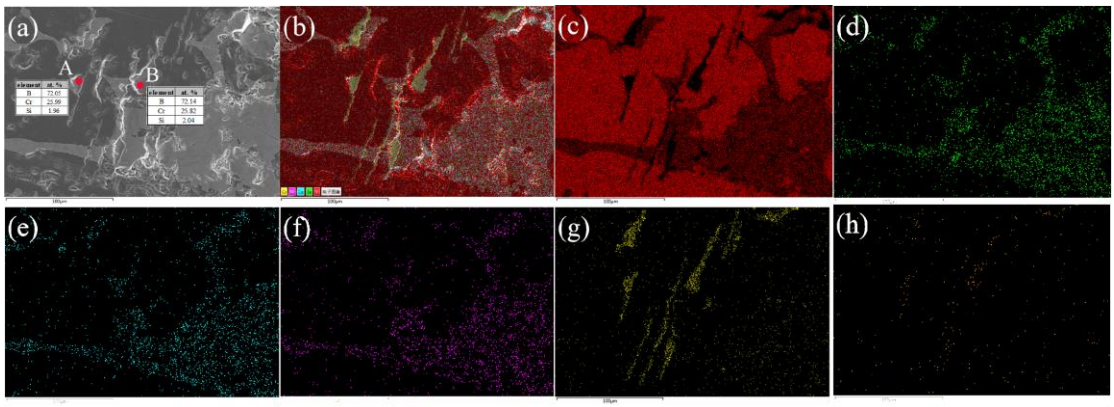

Fig. 3. The EDS results of $CrFeCoNiB_{2.4}$ - Si samples (a) SEM; (b) element mapping; (c) Si; (d) Fe; (e) Co; (f) Ni; (g) Cr; (h) B mapping.

The distribution behavior of B between Si and $CrFeCoNiSi_6$ phases was a key factor to measure the effect of B removal using HEAs solvent. $CrFeCoNiSi_6$ alloy power (Table 1), metallurgical-grade Si powder, and Si-B powder were weighed accurately and proportionally. They were placed in an induction furnace with a power of 75%, and maintained for 2 hours under an Ar atmosphere. The induction coil was slowly moved down using the drawing system, to develop a temperature gradient along the axial direction of the sample.

The greater the amount of B transferred from Si to HEA, the higher the B removal rate, which can be calculated from Eq. (2). A fraction of B that migrated from Si was dissolved in the alloy phase, and the other was precipitated in the form of CrB_x

$$V_B = \left[1 - \left(\frac{C_1}{C_2}\right)\right] \times 100\% \qquad (2)$$

where V_B is the mobility of B which reflects the distribution behavior of B in Si. C_1 and C_2 are the B content in Si after equilibrium and the initial B content in Si, respectively. The initial concentration of B was around 6782 ppmw and 67 ppmw in the Si-B alloy powder and Si powder which were calculated by the ICP-OES.

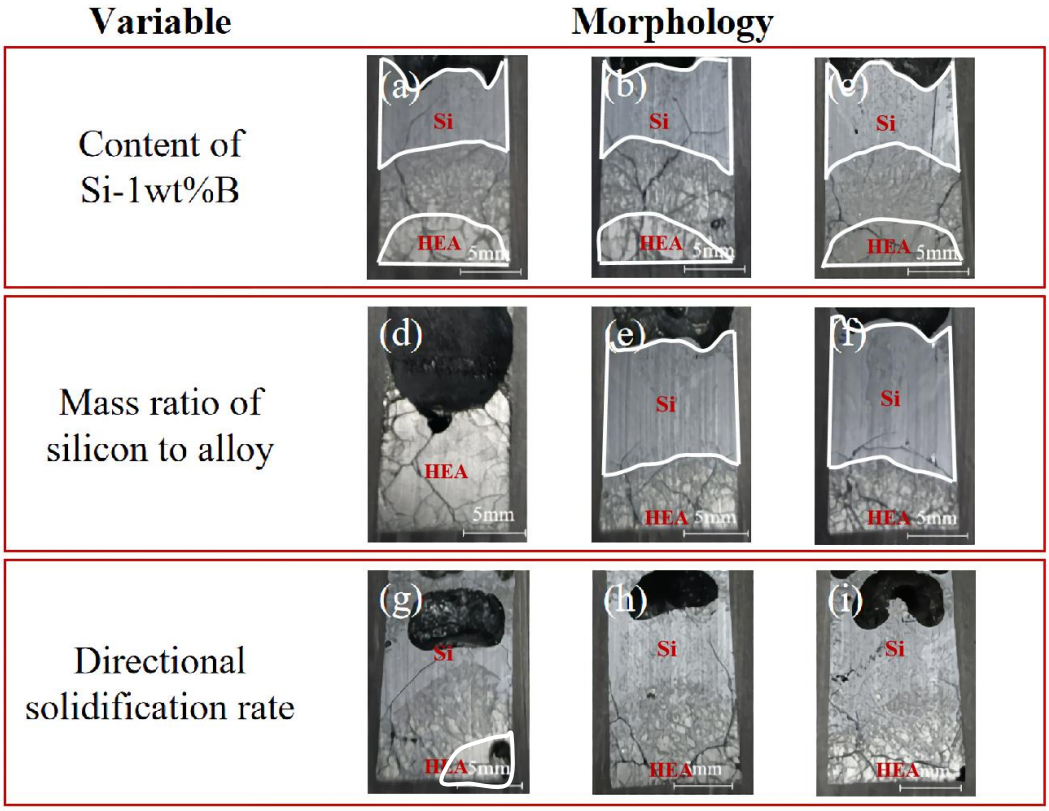

Fig. 4. The cross section of the sample with: different content of Si B powder (a) 10wt% Si B powder; (b) 20wt% Si B powder; (c) 30wt% Si B powder; different mass ratio of Si to alloy (d)mSi/mA=0:1；(e)mSi/mA=2:1；(f)mSi/mA=3:1; different directional solidification rates (g)1mm/h；(h)3mm/h；(i)4mm/h;

The mass ratio of Si to HEAs is 1:1, and the directional solidification rate is 2mm/h in **Figs. 4(a)–(f)**. The pure Si increased with an raise mass ratio of Si to the HEAs. The best separation effect is shown in **Fig. 4(f)**, where the removal efficiency of B increased due to the proportion of Si increased.

The mass ratio of Si to HEAs is 1:1, and the content of Si-1wt%B powder is 20wt.% in **Figs. 4(g)–(i)**. As the directional solidification rate increased, the boundary between Si and the transition region gradually became blurred, and the separation effect became worse. The boundary was clear at the directional solidification rate of 2 mm/h in Fig. 4(g).

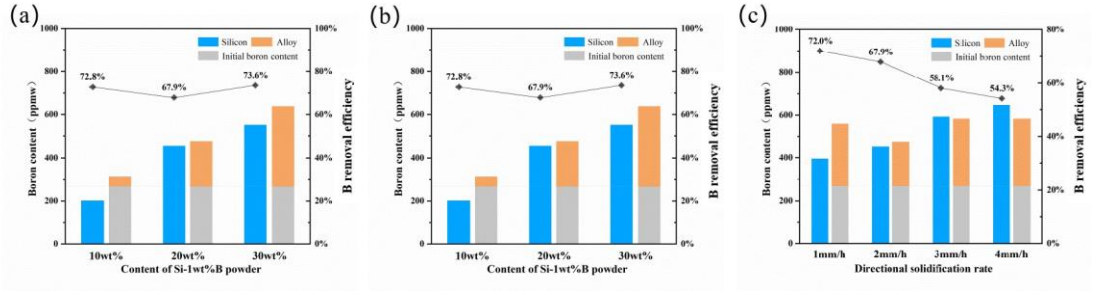

Fig. 5. The effects of B content with the content of Si powder (a), the mass ratio of Si to alloy

(b), and the rate of directional solidification (c)

The amount of B in the Si and alloy increased with the increasing amount of Si-B HEAs powder, yielding the B removal efficiency of ~70%, as shown in **Fig. 5(a)**. There was a little difference in B amount between Si and the HEAs, indicating that B was evenly distributed in Si/HEAs. The reduced amount of B in Si was not equal to the increased amount of B in the HEAs, because excess B formed boride and precipitated at the bottom of the crucible. As the overall amount of B in the system increased, the amount of boride and the equilibrium amount of B in Si also increased.

As the directional solidification rate increased, the amount of B in Si increased and B removal efficiency decreased in **Fig. 5(c)**. The crystallinity of Si during precipitation was better due to the slow directional solidification rate, the impurities were fewer, and the separation effect was better. The B concentration in the HEAs was close to saturation, and the change in the B content in the alloy under various directional solidification rate conditions was not significant.

Si is first precipitation during the solidification due to the higher melting point, so the mole fraction of B in solid ($X_{\text{B in solid}}$) equals that in Si ($X_{\text{B in Si}}$). Accordingly, B in liquid ($X_{\text{B in liquid}}$) equals the that in HEA ($X_{\text{B in HEA}}$). In particular, Si and HEA of equal mass ($m_{Si}=m_{HEA}$) are weighed during ICP analysis. So the segregation coefficient of B (k_B can be expressed as Eq. (3):

$$\ln k_{\text{B}} = \ln \frac{X_{\text{B(s) in solid}}}{X_{\text{B(l) in liquid}}} = \ln \frac{X_{\text{B(s) in solid Si}}}{X_{\text{B(l) in HEA}}} = \ln \frac{\dfrac{m_{B\text{ in Si}} \cdot M_{Si}}{m_{\text{Si}} \cdot M_B}}{\dfrac{m_{B\text{ in HEA}} \cdot M_{HEA}}{m_{HEA} \cdot M_B}} = \ln \frac{m_{B\text{ in Si}} \cdot M_{Si}}{m_{B\text{ in HEA}} \cdot M_{HEA}} \quad (3)$$

In different experiments, the amount of B in Si and HEAs was always shown to be balanced. The mass ratio of B in Si to HEAs was 0.921, and the $k_B \approx 0.066$ (1723 K). The Si-Al alloy system has been widely studied, with the k_B of 0.076 (1073 K), 0.22 (1273 K), and 0.49 (1473 K)[10].The k_B is related to the melting free energy of B in the HEAs, the HEAs temperature, the activity coefficient of B in the HEAs melt ($\gamma^{\circ}_{\text{B in HEAs}}$), and the activity coefficient of solid Si ($\gamma^{\circ}_{\text{B in Si}}$). $\gamma^{\circ}_{\text{B in Si}}$ is only related to the HEAs temperature[11], as shown in Eq. (4):

---

[10] Yoshikawa, T.; Morita, K. Refining of Silicon during Its Solidification from a Si-Al Melt. *J. Cryst. Growth* **2009**, *311 (3)*, 776–779.

[11] Khajavi, L. T.; Morita, K.; Yoshikawa, T.; Barati, M. Thermodynamics of Boron Distribution

$$\ln \gamma^{\circ}_{\text{B in Si}} = (16317 \pm 282) \times \left(\frac{1}{T}\right) - (7.06 \pm 0.18)\,(1483 \sim 1583K) \quad (4)$$

$\gamma^{\circ}_{\text{B in HEAs}}$ is also related to the composition of the melt at a certain temperature. With the precipitation of primary Si, the amount of Si in the melt decreased, and $\gamma^{\circ}_{\text{B in HEAs}}$ raised, resulting in an increase of k_B. This is not conducive to the migration of B from Si.

In summary, the quaternary equimolar CrFeCoNi and Si were found to form the solid-solution phase with an average composition of $CrFeCoNiSi_6$ (HEAs) at high temperatures. The elemental composition of the solid-solution phase remained unchanged for temperatures in the 900-1450 ^{o}C range, and there was Cr-dominated segregation. The solid solubility of B in $CrFeCoNiSi_6$ was ~1600 ppmw. CrB_2 was formed after the B amount in the solid-solution phase reached an upper limit. The B segregation coefficient was ~0.066 in the $CrFeCoNiSi_6$/Si system, lower than that for the traditional Si-Al alloy system. By decreasing the directional solidification rate and the mass ratio of Si to the HEA, the diffusion rate of B increased.

Funding

This work was supported by the International Science and Technology Innovation Cooperation Project of Sichuan Province, China (No. 2021YFH0131); the Sichuan University postdoctoral interdisciplinary Innovation Fund (No. 0030704153019); the Science and Technology Cooperation Program of Sichuan University and Panzhihua City (2021); Key Research and Development Project (No. 2019-YF05-01833-SN

References

in Solvent Refining of Silicon Using Ferrosilicon Alloys. *J. Alloys Compd.* **2015**, *619*, 634–638

Table of Contents：